J Solid State Electrochem (2012) 16:1503–1508
DOI 10.1007/s10008-011-1553-y

ORIGINAL PAPER

$LiFePO_4$/CA cathode nanocomposite with 3D conductive network structure for Li-ion battery

Qiong Jiang · Yunlong Xu · Chongjun Zhao · Xiuzhen Qian · Shaowei Zheng

Received: 4 July 2011 / Revised: 5 September 2011 / Accepted: 9 September 2011 / Published online: 2 October 2011

Abstract A novel $LiFePO_4$/Carbon aerogel (LFP/CA) nanocomposite with 3D conductive network structure was synthesized by using carbon aerogels as both template and conductive framework, and subsequently wet impregnating $LiFePO_4$ precursor inside. The LFP/CA nanocomposite was characterized by X-ray diffraction (XRD), TG, SEM, TEM, nitrogen sorption, electrochemical impedance spectra and charge/discharge test. It was found that the LFP/CA featured a 3D conductive network structure with $LiFePO_4$ nanoparticles ca. 10–30 nm coated on the inside wall of the pore of CA. The LFP/CA electrodes delivered discharge capacity for $LiFePO_4$ of 157.4, 147.2, 139.7, 116.3 and 91.8 mA h g^{-1} at 1 °C, 5 °C, 10 °C, 20 °C and 40 °C, respectively. In addition, the LFP/CA electrode exhibited good cycling performance, which lost less than 1% of discharge capacity over 100 cycles at a rate of 10 °C. The good high rate performances of $LiFePO_4$ were attributed to the unique 3D conductive network structure of the nanocomposite.

Keywords $LiFePO_4$/CA nanocomposite · 3D conductive network structure · Impregnation · High rate performance

Introduction

The olivine $LiFePO_4$ is a promising cathode material for lithium-ion batteries due to its special merits such as natural abundance, excellent cycle stability, inexpensiveness and environmental friendliness, which facilitate its potential applications in the batteries of electric vehicles (EVs) and hybrid electric vehicles (HEVs) [1–4]. In order to fulfill these applications, it is necessary to acquire $LiFePO_4$ composites with good electrochemical performance at high current, which was mainly hindered by the low electronic conductivity (10^{-9} to 10^{-10} S cm^{-1}) [1, 2] and low diffusion rate of lithium ion (1.8×10^{-14} cm^2 s^{-1}) [4]. Many attempts have been made to overcome this problem by minimizing the particles size [5, 6] or coating an electronically conductive layer [7–9]. Recently, some efforts have been made to find an efficient method to reduce the $LiFePO_4$ particles size to nano-scale and coat the $LiFePO_4$ with a conducting layer [10]. Hence, it is crucial to choose a suitable carbon source which simultaneously fulfills this dual function.

Mesoporours carbon with 3D and continuous conductive network structure may be a good candidate. Guo et al. [11] reported the enhancement of conductive mesopores on both Li^+ and e^- migration. Wu et al. [12] reported an improvement of nanoporous carbon matrix on the charge–discharge performance of nanometer particles, but the method suffered from a complicated preparation process. Wang et al. [13] presented the carbon-coated $LiFePO_4$ prepared by a carbon aerogel synthesis process, and the composites exhibited good electronic conductivity. Recently, Doherty et al. [14] presented a meso/macroporous hierachical structure $LiFePO_4$ electrode materials by using a meso/macroporous carbon monolith as template. Very recently, Yang and Gao [15] prepared $LiFePO_4$/C materials by using microporous active carbon and ordered mesoporous carbon CMK-3, which was prepared by using ordered mesoporous silica molecular sieve as the template and the sucrose as the carbon source, as template.

Q. Jiang · Y. Xu (✉) · C. Zhao · X. Qian · S. Zheng
Key Laboratory for Ultrafine Materials of Ministry of Education, Shanghai Key Laboratory of Advanced Polymeric Materials, School of Materials Science and Engineering, East China University of Science and Technology, Shanghai 200237, China
e-mail: xuyunlong@ecust.edu.cn

To extend the work cited above, in this study we report a facile impregnation method to prepare a $LiFePO_4$/carbon aerogel (LFP/CA) nanocomposite with 3D conductive structure by using CA as a template and conductive framework. The templating function of CA can be attributed to its unique properties, such as the 3D connectivity of the pore system, high pore volume and narrow pore size distribution, which can control the particle size of $LiFePO_4$ and the morphology of LFP/CA nanocomposite. The conductive framework function of the CA can be attributed to the continuous and connected nano carbon particles. The detailed structure and the electrochemical performance of LFP/CA nanocomposite were evaluated.

Experimental

Preparation of the LFP/CA nanocomposite

The CA was prepared through a sol–gel method as reference [16]. Subsequently, after the grinding and sifting process, CA was chemically oxidized by nitric acid for 2 h under certain temperature to enhance its hydrophility. Stoichiometric amounts of $Fe(NO_3)_3{\cdot}9H_2O$ (Sinopharm Chemical Reageni Co. Ltd, AR) and LiH_2PO_4 (Shanghai China Lithium Industrial Co. Ltd, GR) were dissolved in de-ionized water to form a saturated solution at room temperature. Then the CA was impregnated with the above solution and filtrated until incipient wetness was obtained. The impregnated sample was first dried under the irradiation of an infrared light for 12 h and then calcined at 600 °C for 3 h (2 °C min^{-1}) under a reductive atmosphere (90% Ar and 10% H_2).

Characterization

The crystal structures of the sample were characterized by X-ray diffraction measurement (XRD, D/MAX 2550 V, Japan) using Cu Kα radiation (λ=0.154 nm). The morphologies were evaluated by field emission transmission electron microscopy (FETEM, JEM-2010 F Japan) and field emission scanning electron microscopy (FESEM, Hitachi S-4800, Japan). The surface areas and pore volumes of samples were determined via nitrogen sorption with the Micromeritics Tristar surface area and porosity analyzer (BET, BJH, TriStar 3000, American). The surface area and pore volumes were calculated using the Brunauer–Emmet–Teller (BET) method and the Barrett–Joyner–Halenda (BJH) method, respectively. The carbon content of the LFP/CA nanocomposite was evaluated by thermogravimetry (SDT Q600, Switzerland) at a heating rate of 10 °C min^{-1} from ambient temperature to 800 °C in air.

Electrochemical characterization

Study of the electrochemical properties of LFP/CA and CA was performed by assembling 2032 coin cells. The electrodes were prepared by dispersing 80 wt.% active material, 10 wt.% acetylene black (AB, Shanghai Haohua Chemical Co. Ltd) and 10 wt.% polyvinylidene fluoride (PVDF; Shanghai Ofluorine Chemical Technology Co. Ltd) binder in *N*-methyl-2-pyrrolidon (NMP; Shanghai Lingfeng Chemical Reagent Co. Ltd) to form a homogeneous slurry. The slurry was then uniformly spread onto a thin aluminum foil, and dried in a vacuum oven at 120 °C for 10 h. The cells were assembled in an argon-filled glove box (Super1220/750) using lithium metal as anode electrode, Cellgard 2400 as the separator, 1 M $LiPF_6$ in ethylene carbonate (EC) and diethyl carbonate (DMC) (1:1 by volume) as the electrolyte. The charge–discharge characteristics and cycling performance test were recorded under different current densities in the voltages of 2.5–4.2 V (vs. Li/Li^+) at room temperature. The electrochemical impedance spectroscopy (EIS) was performed by using impedance analyzer (RST5200) in the frequency range of 10^5–10^{-2} Hz. The LFP/CA was used as the working electrode and the lithium as the counter electrode.

Results and discussion

XRD pattern and TG of LFP/CA nanocomposite

Figure 1 shows the XRD patterns of LFP/CA nanocomposite and CA, as well as the JCPDS of normal $LiFePO_4$, respectively. Figure 1 clearly shows that all intense diffraction peaks for LFP/CA can be well indexed

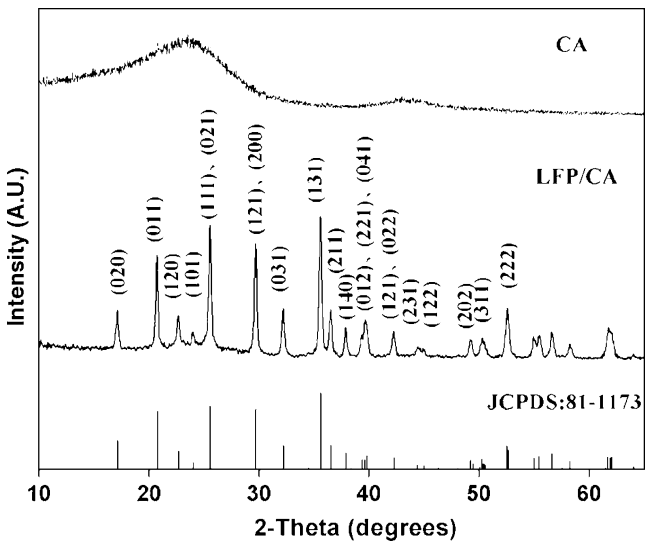

Fig. 1 XRD patterns of the LFP/CA nanocomposite and CA

to orthorhombic $LiFePO_4$. Moreover, except those of $LiFePO_4$, no other peaks appeared; therefore, it is confirmed that pure $LiFePO_4$ was formed through this preparation process. The slight bump between 20° and 35° in the XRD pattern of LFP/CA originates from the amorphous CA, which is consistent with the broad peak in the range of 20–35° of the XRD pattern for CA.

The carbon content of the LFP/CA nanocomposite was further determined by TG technique, shown in Fig. 2, and a total weight loss of 37 wt.% was clearly seen. Since the $LiFePO_4$ can be oxided to $Li_3Fe_2(PO_4)_3$ or Fe_2O_3 in the temperature range of 300–400 °C at air atmosphere, which gains a weight ratio of ca. 5 wt.% [17]. The carbon content was calculated to be 42 wt.%.

SEM and TEM images of LFP/CA nanocomposite

Figure 3 shows the SEM images of the CA and LFP/CA nanocomposite. Compared with CA (Fig. 3a), it is obvious that the pores or gaps between neighbor particles decrease, and at the same time, the particles of LFP/CA (Fig. 3b) become bigger. Since no bared $LiFePO_4$ particles were observed, it is concluded that the pores or gaps in the CA were occupied by the formed $LiFePO_4$ particles. Thus, the change in morphology can be explained as follows: The porous CA provided a framework into which the $LiFePO_4$ can impregnate. The TEM result of LFP/CA (Fig. 4a) shows that the $LiFePO_4$ nanoparticles ca. 10–30 nm is coated on a continuous CA conductive framework and this structure favors the diffusion of Li^+ and e^- (Fig. 4b).

N_2 isothermal and BET of LFP/CA nanocomposite

Figure 5 shows the N_2 adsorption/desorption isotherms for the CA and the LFP/CA nanocomposite, which can further confirm the impregnation of $LiFePO_4$ in CA inner pores.

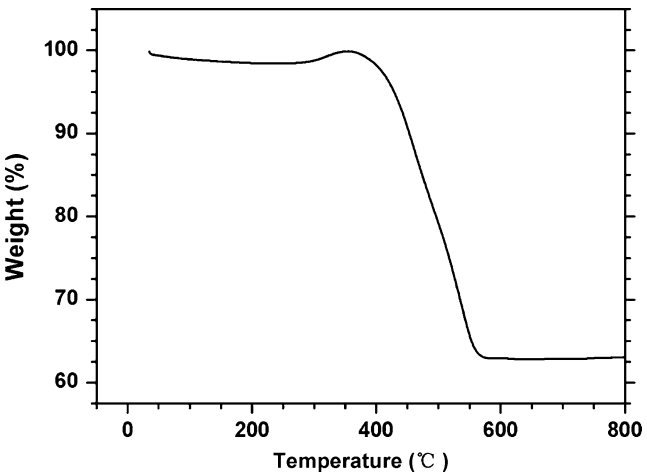

Fig. 2 TG curve of the LFP/CA nanocomposite

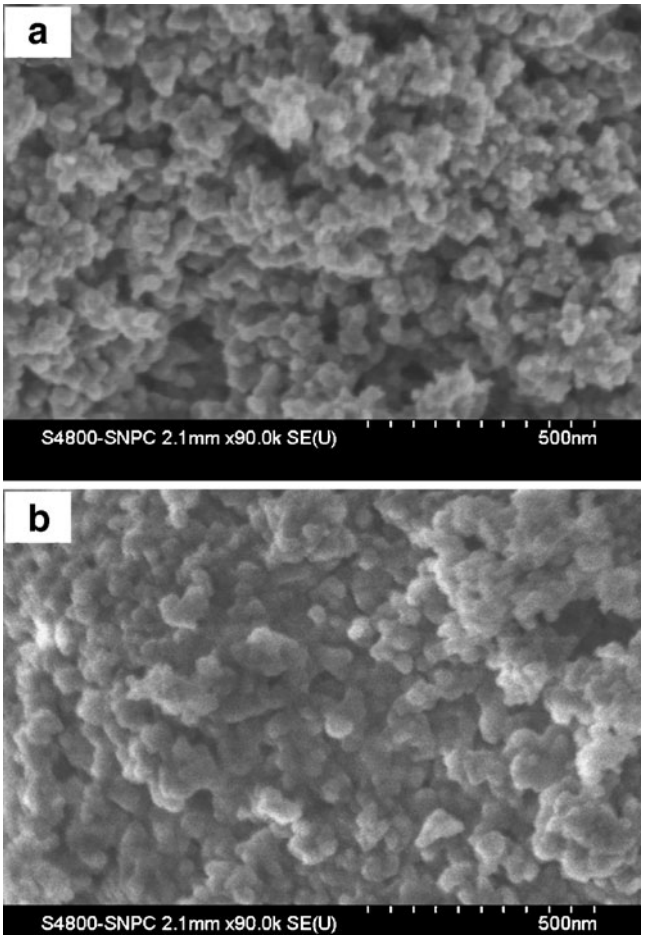

Fig. 3 SEM images of CA (**a**) and the LFP/CA nanocomposite (**b**)

All the N_2 sorption isotherms are typical type IV isotherms with hysteresis loops, indicating that both CA and LFP/CA nanocomposite have mesoporous structure. Furthermore, the inflection point in the isotherm for LFP/CA showing a shift to a smaller relative pressure proves that the mesopore of CA is filled or blocked by $LiFePO_4$, resulting in a reduced surface area and pore volume. Table 1 shows that the BET surface area and pore volumes dropped from 278 $m^2\ g^{-1}$ and 0.85 $cm^3\ g^{-1}$ for CA to 243 $m^2\ g^{-1}$ and 0.46 $cm^3\ g^{-1}$ for LFP/CA nanocomposite due to the filling of pores after $LiFePO_4$ impregnate.

Electrochemical performances of LFP/CA nanocomposite

In order to determine the electrochemical performance of the LFP/CA nanocomposite, the charge–discharge tests of the LFP/CA nanocomposite electrode at different rates were performed. When we calculated the current and discharge capacity, the used mass was only from the active $LiFePO_4$ and the carbon mass was subtracted. Figure 6a shows the superior cycling performance of the LFP/CA nanocomposite at various current rates, and the discharge capacity loss

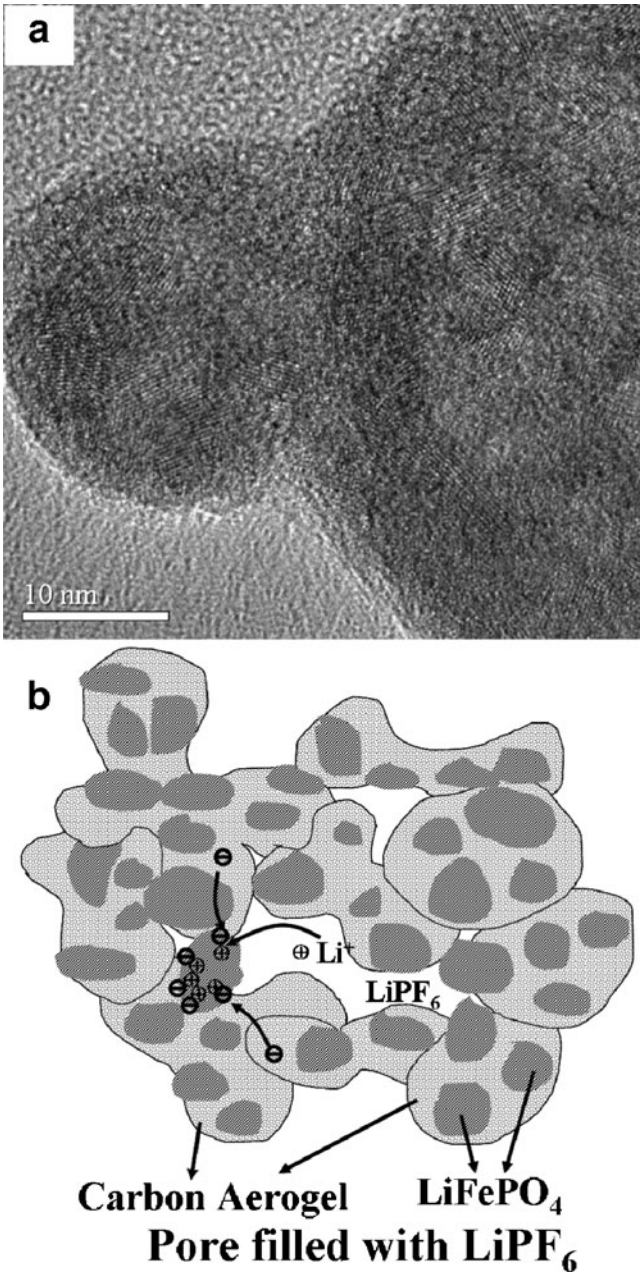

Fig. 4 HRTEM image of LFP/CA nanocomposite (**a**) and schematic illustration (**b**)

is less than 1% over 100 cycles even at the rate of 10 °C. Figure 6b displays the initial discharge profiles of the sample under different current rate between 2.5 and 4.2 V (vs. Li/Li^+), showing the outstanding high capacity and high rate performance. At low current rate of 1 °C, the discharge capacity is 174 mA h g^{-1}, which even exceeded the theoretical capacity of $LiFePO_4$ (170 mA h g^{-1}). Although the capacity decreases with the discharge rate increasing, the electrode still delivers a capacity of 102.37 mA h g^{-1} at a high discharge rate up to 40 °C (1.5 min). As shown in Fig. 6c, the discharge capacity of

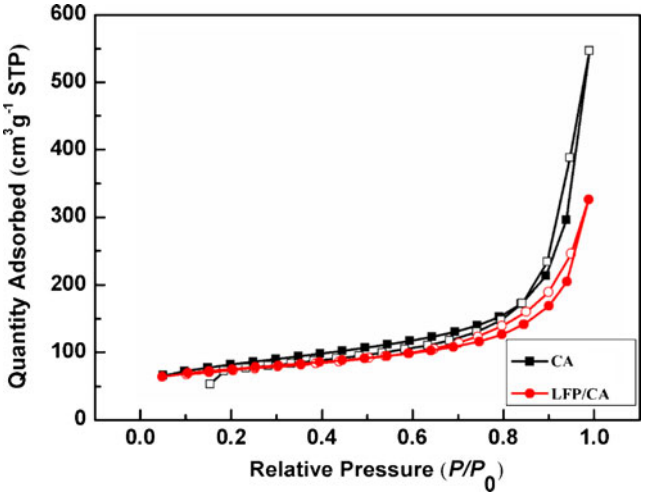

Fig. 5 Nitrogen adsorption/desorption isotherms of CA and LFP/CA nanocomposite

CA is 24.7 and 16 mA h g^{-1} at 1 °C and 10 °C, respectively. This capacity may attributed to the interfacial adsorbing/desorbing of PF_6^- in porous carbon aerogels process [15]. Considering that the CA content of LFP/CA nanocomposite is 42 wt.%, the capacity of pure $LiFePO_4$ can be calculated, which are 157.4, 147.2, 139.7, 116.3 and 91.8 mA h g^{-1} at 1 °C, 5 °C, 10 °C, 20 °C and 40 °C, respectively.

Further study of the charge–discharge curves of LFP/CA is necessary to understand why $LiFePO_4$ in LFP/CA nanocomposite has good high capacity and high rate performance. The discharge profiles can be divided into two parts as shown in Fig. 6b, the plateau part (I) and the sluggish slope part (II), corresponding to different mechanisms. The plateau region represents the biphasic reduction reaction in the bulk between $FePO_4$ and $LiFePO_4$ [12]. The short Li^+ diffusion distance preserves an efficient Li^+ insection/extraction process from the bulk of the $LiFePO_4$ electrode at high current rates or within a short discharge–charge time. The slope part may contribute to the surface Li storage for the high surface area of LFP/CA [12]. The slope part can be seen in many other electrode materials [14, 18–21]. Jiang et al. [22, 23] found that the capacity from the surface Li storage was very stable upon cycling or increasing the discharge/charge current densities. The surface Li storage only depends on the surface area, and not on the diffusion time. Thus, it plays a very important role on the high rate performance and cycle ability.

Table 1 Pore volumes and BET surface areas of CA and the LFP/CA nanocomposite

Sample	S_{BET} (m^2 g^{-1})	Pore volumes (cm^3 g^{-1})
CA	278	0.85
LFP/CA	243	0.46

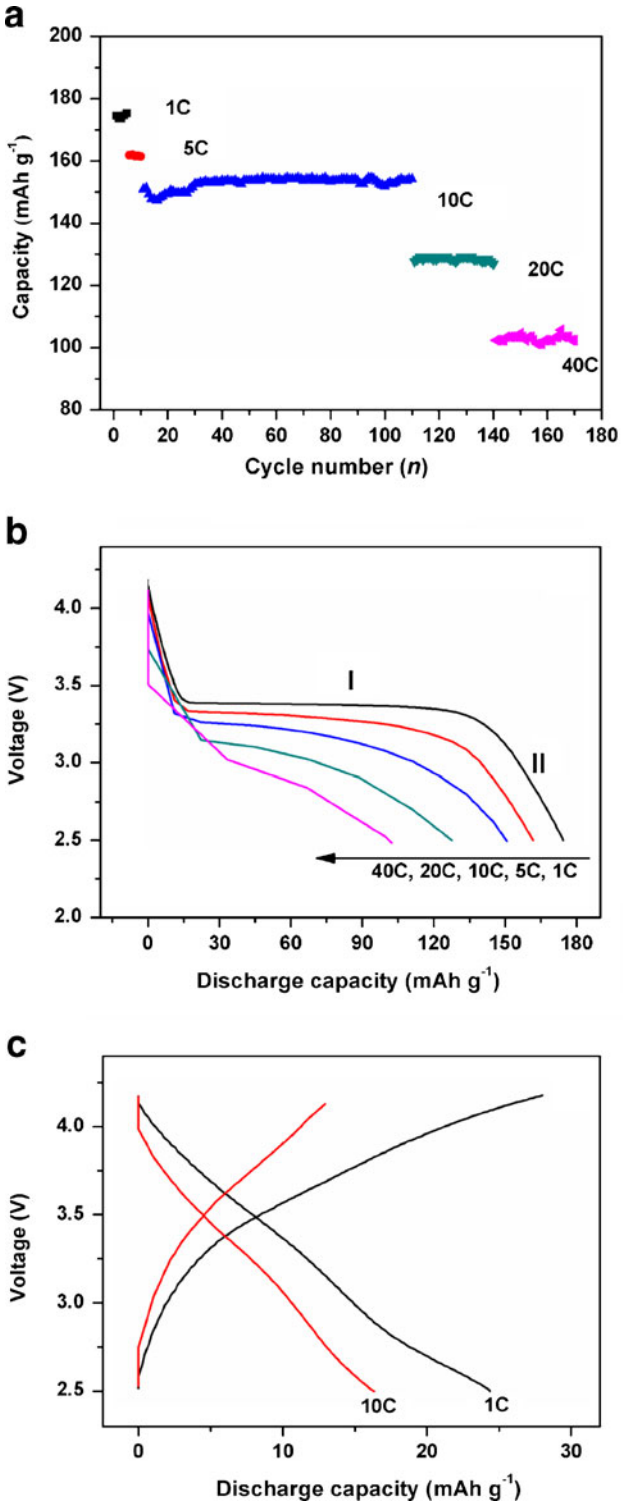

Fig. 6 **a** Cycling performance of LFP/CA cathode at different rates between 2.5 and 4.2 V (vs. Li^+/Li). **b** Discharge curves of LFP/CA cathode at different rates. **c** Charge/discharge curves of CA cathode at different rates

Figure 7 shows the EIS test results of LFP/CA nanocomposite cell. The EIS measurement was measured after 10 cycles with different current rates of 1 °C, 10 °C and 40 °C, respectively. The charge transfer resistance R_{ct} (semicircle in the middle frequency range) changed little, suggesting that electrode structure was not significantly destroyed even at high current rate, which is consistent with the results in the discharge performance mentioned above.

From the inclined lines in the Warburg region, the Li^+ diffusion coefficient may be estimated using the following equation [24]:

$$D = (R^2T^2)/(2A^2n^4F^4C^2\sigma^2) \quad (1)$$

where R is the gas constant, and T, A, n, F and C are the absolute temperature, the surface area of the cathode, the number of electrons per molecule during oxidization, the Faraday constant, the concentration of Li^+ and δ the Warburg factor associated with Z_{re}, respectively.

$$Z_{re} \propto \sigma\omega^{-1/2} \quad (2)$$

From Eq. 2, the Warburg factor could be obtained by linear fitting the relation plot between Z_{re} and reciprocal square root of the angular frequency (as shown in the insection part of Fig. 7). In Fig. 7, it can be concluded that the Li^+ diffusion coefficient increased when the current was increased, which may be due to the SEI film formed with higher formation current density which has relatively higher ionic conductivity [25]. The results can also explain the good performance of LFP/CA cathode at high current rate.

Obviously, the involvement of CA enhances both the discharge capacities and stable cycling properties, which maybe correlate with the following effects of CA on $LiFePO_4$: (a) The network of CA confined the formation and growth of $LiFePO_4$ particle, hence $LiFePO_4$ particles in nano-scale was formed which facilitate the diffusion of Li^+. (b) The CA serves as a conducting 3D network, which

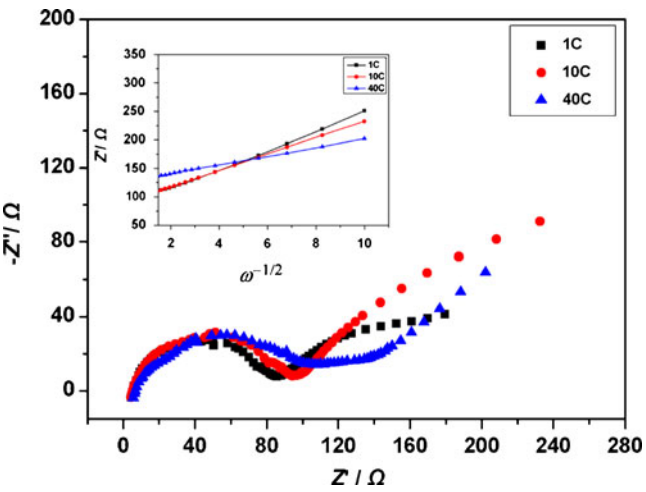

Fig. 7 EIS of LFP/CA cell after ten cycles at the rate of 1 °C (**a**), 10 °C (**b**) and 40 °C (**c**). *Inset*: variations and fittings between Z_{re} and reciprocal square root of the angular frequency at low frequency region of LFP/CA cell

enables e^- to migrate. (c) As the $LiFePO_4$ nanoparticle was well covered with CA, aggregation during preparation and the subsequent charge/discharge process was efficiently inhabited. (d) The LFP/CA nanocomposite exhibits abundant pores to hold electrolyte and a high special surface area of up to 243 $m^2\ g^{-1}$ enabling the active materials to full contact with electrolyte, hence improving the utilization ratio of the material. (e) The mesopore of the nanocomposite can release the strain on/from $LiFePO_4$ during the Li^+ insertion/extraction process, especially at high rate discharge. (f) The excellent high rate performance of the electrodes may be partially ascribed to the low specific current density of the active material because of the large surface area and 42 wt.% CA coating, which can effectively stabilize the electrode and preserve a high capacity at the high rate.

Conclusion

In summary, a novel 3D conductive network structure of $LiFePO_4$/CA (LFP/CA) nanocomposite for lithium-ion battery was synthesized by using continuous carbon aerogels as both template and conductive framework. The LFP/CA electrodes delivered discharge capacity for $LiFePO_4$ of 157.4, 147.2, 139.7, 116.3 and 91.8 mA h g^{-1} at 1 °C, 5 °C, 10 °C, 20 °C and 40 °C. Furthermore, the discharge capacity loss is less than 1% over 100 cycles at rate of 10 °C. Above all, this LFP/CA nanocomposite is ideal as an electrode material for high-power lithium batteries. The excellent electrochemical performances are attributed to the unique 3D conductive network structure, the very small particle size, the improved conductivity provided by CA, as well as larger contacted area between the electrolyte and the nano $LiFePO_4$ particles.

Acknowledgements The work was partially supported by Shanghai Nanotechnology Promotion Center (Grant NO. 0852 nm02300) and Shanghai International Science and Technology Cooperation Foundation (Grant No. 08230705600)

References

1. Padhi AK, Nanjundaswarmy KS, Goodenough JB (1997) J Electrochem Soc 144:1188–1194
2. Xu YN, Chung SY, Blocking JT, Chiang YM, Ching WY (2004) Electrochem Solid-State Lett 7(6):A131–A134
3. Recham N, Dupont L, Courty M, Djellab K, Larcher D, Armand M, Trascon JM (2009) Chem Mater 21:1096–1107
4. Prosini PP, Lisi M, Zane D, Pasquali M (2002) Solid State Ionics 148:45–51
5. Lim S, Yoon CS, Cho J (2008) Chem Mater 20:4560–4564
6. Meligrana G, Gerbaldi C, Tuel A, Bodoardo S, Penazzi N (2006) J Power Sources 160:516–522
7. Ni JF, Morishita M, Kawabe Y, Watada M, Takeichi N, Sakai T (2010) J Power Sources 195:2877–2882
8. Yang Y, Liao XZ, Ma ZF, Wang BF, He L, He YS (2009) Electrochem Commun 11:1277–1280
9. Hu YS, Guo YG, Dominko R, Gaberscek M, Jamnik J, Maier J (2007) Adv Mater 19:1963–1966
10. Huang H, Yin SC, Nazar LF (2001) Electrochem Solid-State Lett 4:A170–A172
11. Guo YG, Hu YS, Sigle W, Maier J (2007) Adv Mater 19:2087–2091
12. Wu XL, Jiang LY, Cao FF, Guo YG, Wan LJ (2009) Adv Mater 21:2710–2714
13. Wang GX, Yang L, Bewlay SL, Chen Y, Liu HK, Ahn JH (2005) J Power Sources 146:521–524
14. Doherty CM, Caruso RA, Smarsly BM, Adelhelm P, Drummond CJ (2009) Chem Mater 21:5300–5306
15. Yang M, Gao QM (2011) J Alloys Compd 509:3690–3698
16. Mirzaeian M, Hall PJ (2009) Electrochim Acta 54:7444–7451
17. Lou XM, Zhang YX (2011) J Mater Chem 21:4156–4160
18. Balaya P, Li H, Kienle L, Maier J (2003) Adv Funct Mater 13:621–625
19. Wang YG, Wang YR, Hosono E, Wang KX, Zhou HS (2008) Angew Chem Int Ed 47:7461–7465
20. Chen SY, Gao B, Su LH, Mi CH, Zhang XG (2009) J Solid State Electrochem 13:1361–1366
21. Hu YS, Kienle L, Guo YG, Maier J (2006) Adv Mater 18:1421–1426
22. Jiang CH, Wei MD, Qi ZM, Kudo T, Honma I, Zhou HS (2007) J Power Sources 166:239–243
23. Jiang CH, Honma I, Kudo T, Zhou HS (2007) Electrochem Solid-State Lett 5:A127–A129
24. Zhou YK, Wang J, Hu YY, O'Hayre R, Shao ZP (2010) Chem Commun 46:7151–7153
25. He YB, Li BH, Yang QH, Du HD, Kang FY, Ling GW, Tang ZY (2010) Effects of current densities on the formation of $LiCoO_2$/graphite lithium ion battery. J Solid State Electrochem